Optically driven spin nutations in the ground state of atomic sodium

Dieter Suter, Martin Rosatzin, and Jiirgen Mlynek
Institute of Quantum Electronics, Swiss Federal Institute of Technology (ETH) Zürich, CH-8093 Zürich, Switzerland
(Received 8 August 1989)

We report detailed studies of the dynamic response of spin coherence to a step input of optically resonant narrow-band laser radiation in the presence of a static transverse magnetic field. The evolution of the spins is observed with a cw optical probe beam using polarization-selective detection of the transmitted light. In extension of previous optical-pumping experiments, the dynamics of the system are studied systematically as a function of optical-resonance detuning and intensity. Our experiments are performed on the $3s\ ^2S_{1/2}$ ground state of sodium, using the D_1 line for optical excitation. The experimental-data are compared with theoretical predictions based on a Bloch-type equation of motion for an optically driven spin system in a $J=\frac{1}{2}$ ground state.

I. INTRODUCTION

Transfer of angular momentum from photons to electrons is an efficient way of polarizing the spins of atomic systems to values near unity.[1] The spin polarization generated in the system can be observed as magnetization, using, e.g., pickup coils,[2] or optically, by measuring the response of the sample to polarized light.[1] These purely optical studies of spin systems can be performed either in the frequency domain under steady-state conditions or in the time domain, using pulsed light for excitation.[1,3] In the present work we are interested in the transient dynamics of optically driven electron spins in a magnetic field. We revisit transverse optical pumping at the example of sodium atoms, using narrow-band laser radiation for excitation. The optical pumping generates a coherent superposition of the magnetic substates which evolves under the combined influence of the magnetic and optical fields. This evolution can be interpreted as optically induced spin nutation which we observe with polarization selective detection of a cw optical probe beam.

The motivation for this study is twofold. On one hand, we are interested in the dynamics of radiation-coupled three-level systems; here the special situation is analyzed where two states are sublevels of an electronic ground state. On the other hand, we are interested in the development of purely optical methods to study magnetic resonance phenomena. In both respects, our study is closely related to quantum-beat spectroscopy using a pump-probe technique;[4] we analyze the preparation stage of such a quantum-beat experiment, including the limit of long-pulse excitation.

In contrast to most previous work,[3,4] our experiment is not restricted to the limit of optical broadband excitation and impact excitation.[5] In our investigations, a step input of ***intense*** and ***narrow-band*** laser light is used to excite the atomic sublevel coherence; we continue the observation of the system until the initial sublevel transient has decayed and a steady state is reached. This excitation process determines also amplitude and phase of the quantum-beat signal or "free induction decay," which can be observed after the laser light is switched off.[6] We study the initial transient as a function of the optical resonance detuning which determines the signal shape via optical-pumping and light-shift effects; in this respect, our work extends earlier experimental studies of Zeeman light shifts in weak magnetic fields using conventional light sources.[7] Finally, saturation effects of the initial sublevel transient are analyzed.

Our work also yields useful information for experiments where a sequence of excitation pulses is used to induce sublevel coherence.[8] In the case of a two-pulse excitation, e.g., a sublevel echo can be observed for inhomogeneously broadened sublevel transitions.[5,9] It turns out that light-shift effects play a crucial role in the formation of this type of echo; intensity and detuning of the laser radiation are therefore important parameters in such an experiment.[6] The study of the response of atomic multilevel systems to single-pulse laser excitation, as discussed in the present work, is thus an important prerequisite for the understanding of transient phenomena showing up in the case of multiple-pulse excitation.

In Sec. II we introduce the experimental principle and the theoretical model used for the description of our experiment. In Sec. III we develop the theory which is based on a Bloch-type equation of motion for the ground-state polarization. With this approach, simple analytical solutions can be derived which allow an easy visualization of the dynamics of the optically driven spin system in three-dimensional space. In Sec. IV the detector signal is calculated and in Sec. V our experimental results on the various effects of the pump beam, like polarization of the ground state, light shifts, and relaxation, are presented and compared to our theoretical predictions. Finally, we discuss our experimental findings in relation to previous work on spin nutation phenomena in atomic two- and three-level systems.

II. PRINCIPLE OF EXPERIMENT

In order to introduce the basic idea behind our experiment, we consider the model system depicted in Fig. 1. Part (a) shows a schematic representation of the atomic level system considered in our experiment, while part (b)

summarizes the experimental setup. The ground and excited state of our model system are both $J=\frac{1}{2}$ states. We have chosen the propagation direction of the laser beam as the quantization axis. If the pump beam (solid line) is right circularly polarized, it can induce transitions only between the states $|1\rangle$ and $|4\rangle$, thereby depleting the $m_J=-\frac{1}{2}$ ground state. Thus a population difference between the two magnetic substates of the atomic ground state is created by optical pumping. This population difference leads to different absorption and dispersion for left and right circularly polarized light which can be detected by another laser beam. For this probe beam, it is advantageous to choose linearly polarized light, which can be thought of as a superposition of equal amounts of left and right circularly polarized light (dashed line). These circularly polarized components act as probes for the optical transitions with $m_{J'}-m_J=\pm 1$.

The magnetic moment associated with the transition between the Zeeman substates couples also to an external magnetic field B. In our experiment, we apply a static magnetic field perpendicular to the laser beam. In a quantum-mechanical picture, this field generates a coherent superposition of the two substates and leads to an oscillatory exchange of population which can be observed in the polarization selective detection of the optical transitions connected to these sublevels. In a semiclassical picture, the population difference generated by the optical-pumping process corresponds to a macroscopic magnetization m which is forced into precession by the transverse magnetic field.

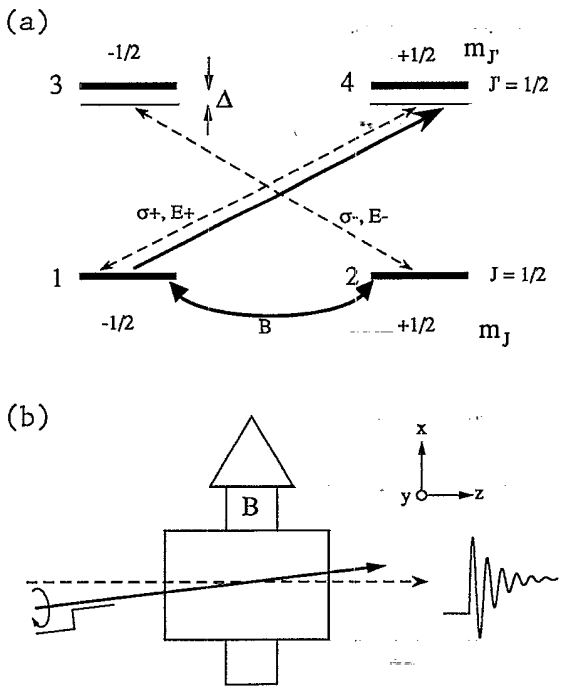

FIG. 1. (a) Schematic representation of the $J=\frac{1}{2}-J'=\frac{1}{2}$ system coupled to the optical fields. The quantization axis is chosen parallel to the propagation direction of the laser beam, so that the atomic substates remain degenerate, even in the presence of a transverse magnetic field *B*. In this representation, the magnetic field induces transitions between the substates, indicated by the curved line. (b) Schematic: representation of the experimental setup. The rectangular box in the center represents the atomic vapor cell in the magnetic field *B*. A pulsed, circularly polarized laser beam (solid line) is used to excite the spin nutation and a cw laser beam (dashed line) is used for detection of the resulting transient spin polarization.

III. SPIN DYNAMICS

The four-level system shown in Fig.1(a) will serve as the prototype system for the description of our experiment. Levels $|3\rangle$ and $|4\rangle$ belong to an electronically excited state, while levels $|1\rangle$ and $|2\rangle$ are substates of the electronic ground state. The z axis (quantization axis) of the coordinate system is parallel to the propagation direction of the laser beam. The laser frequency is tuned close to the optical transition. If the laser field has σ_+ polarization, it couples to the $|1\rangle\leftrightarrow|4\rangle$ transition. It excites, therefore, only atoms that are in the $m_J=-\frac{1}{2}$ state, while spontaneous emission processes populate both ground states; via successive pumping cycles, it is thus possible to pump all the population from state $|1\rangle$ into $|2\rangle$. Population difference between these substates corresponds to a magnetic dipole moment μ_M parallel to the laser beam, and coherence between them to a magnetic dipole in a plane orthogonal to the beam direction. It is therefore helpful to introduce a polarization vector m by the definition

$$\mathbf{m}=(\rho_{12}+\rho_{21},-i(\rho_{12}-\rho_{21}),\rho_{22}-\rho_{11}) , \tag{1}$$

where ρ is the density operator of the system. Population difference is then described by the z component of the polarization vector, while coherence between the two states contributes the x and y components. This corresponds to the usual Feynman-Vernon-Hellwarth parametrization of a quantum-mechanical two-level system;" in our case, however, the vector **m** has also a direct physical interpretation: it is proportional to the macroscopic magnetization associated with the transition $|1\rangle\leftrightarrow|2\rangle$. This magnetization can couple to an external magnetic field; in our experiment, we apply a static field B orthogonal to the direction of the laser beam. We can therefore choose the x axis of our coordinate system parallel to the magnetic field direction. The matrix elements of the magnetic dipole coupling contribute then only off-diagonal elements to the Hamiltonian.

If the dephasing time of the optical transition is short and the relaxation of the excited-state populations is fast enough, it is possible to separate the optical from the spin degrees of freedom.[11] The physical assumption behind this procedure is that the motion of the spins is slow compared to the motion of the electrons. It is then possible to adiabatically eliminate the optical coherences. For small laser intensities, the population of the excited state can be neglected so that only the ground-state sublevels have to be retained. The resulting Hamiltonian depends only on the spin degrees of freedom, but includes a term that shifts the energy of the magnetic substates by an amount that depends parametrically on the laser field. The effect of the laser field can be parametrized with the optical pump rate[11]

$$P_+ = \frac{|\beta_+|^2}{\Gamma_2(1+\bar{\Delta}^2)}, \quad (2)$$

where $\beta_+ = \mu_e E_+ / 2\hbar$ represents the optical Rabi frequency and

$$\bar{\Delta} = \frac{\Delta}{\Gamma_2} \quad (3)$$

denotes the detuning A of the laser frequency from exact resonance, normalized to the half-width at half-height Γ_2 of the optical resonance line; positive $\bar{\Delta}$ corresponds to blue detuning. μ_e is the electric dipole moment of the transition $|1\rangle \leftrightarrow |4\rangle$ and $E+$ describes the electrical field amplitude of the pump pulse. The equation of motion of the ground-state system can now be written as[11]

$$\dot{\mathbf{m}} = \boldsymbol{\Omega} \times \mathbf{m} - \gamma_{\text{eff}} \mathbf{m} + \mathbf{P}, \quad (4)$$

with

$$\boldsymbol{\Omega} = (\Omega_L, 0, \bar{\Delta} P_+), \quad \Omega_L = \frac{\mu_B g B}{\hbar}, \qquad \mathbf{P}(0,0,P_+), \quad \gamma_{\text{eff}} = \gamma + P_+ . \quad (5)$$

Here μ_B denotes Bohr's magneton and g is the Landé factor.

The first term in Eq. (4), $\boldsymbol{\Omega}$ X m corresponds to a precession of the magnetic moment around the effective field $\boldsymbol{\Omega}$ whose x component Ω_L is determined by the strength of the magnetic field B and whose z component results from the term $\bar{\Delta} P_+$. Note that this term is proportional to the laser intensity and shows a dispersionlike behavior. With our choice of coordinate system, the effective field is thus always in the xz plane. The second term in Eq. (4) represents the relaxation of the polarization vector; we have separated the contributions into two parts; a laser-independent term γ, which describes the diffusion of the atoms through the laser beam, and the pump term P_+, which takes the destruction of coherence by the pumping process into account. P_+ is proportional to the laser intensity and the optical-absorption profile. The third term represents the addition of polarization by the optical-pumping process.

The optical pumping has a twofold effect onto the spin system: via transfer of angular momentum from the electromagnetic field into the spin system, it generates a macroscopic magnetic moment at a rate P_+. At the same time, the interaction between the laser field and the atomic system leads to a shift of the energy levels adjacent to the optical transition coupled to the electromagnetic field by an amount $\bar{\Delta} P_+$. This so-called light shift arises from a mixing of ground and excited states by the off-resonant irradiation.[7] Since only one of the substates is being irradiated, the degeneracy between the two ground-state levels is lifted. For the spin system, this energy-level shift looks like a longitudinal magnetic field of strength $\bar{\Delta} P_+$ (in frequency units). In the case of broadband resonant light excitation, the influence of this light-shift term on the dynamics of $\mathbf{m}(t)$ is generally neglected.[12]

The first two terms of Eq. (4), are exactly analogous to the well-known Bloch equation[13] describing the precession of a spin in a magnetic field, except that the magnetic field lies in the xz plane, while the Bloch equations are usually written with the magnetic field along the z axis. Since there is no driving ac field and the relaxation rates of all three components are equal, this change of direction corresponds to a trivial rotation of the coordinate system around the y axis. The solutions of the Bloch equations are well known in this case and correspond to a precession of the magnetization vector around the effective field, damped with the relaxation rate γ_{eff}.

The third term in Eq. (4) represents a source of magnetization which makes the equation of motion inhomogeneous; we will therefore refer to Eq. (4) as the inhomogeneous Bloch equation. The general solution of this equation is

$$\mathbf{m}(t) = \sum_{i=-1}^{1} c_i \xi_i e^{\lambda_i t} + \mathbf{m}_\infty , \quad (6)$$

where the eigenvectors ξ_i and eigenvalues λ_i are given as

$$\xi_0 = (\Omega_L, 0, \bar{\Delta} P_+), \ \lambda_0 = -\gamma_{\text{eff}} , \qquad \xi_{\pm 1} = (\bar{\Delta} P_+, \pm i\Omega, -\Omega_L), \quad \lambda_{\pm 1} = \pm i\Omega - \gamma_{\text{eff}} , \quad (7)$$

with

$$\Omega = (\Omega_L^2 + \bar{\Delta}^2 P_+^2)^{1/2} , \quad (8)$$

and the stationary value is

$$\mathbf{m}_\infty = \frac{P_+}{\gamma_{\text{eff}}(\Omega_L^2 + \bar{\Delta}^2 P_+^2 + \gamma_{\text{eff}}^2)} \times (\bar{\Delta} P_+ \Omega_L, -\gamma_{\text{eff}} \Omega_L, \bar{\Delta}^2 P_+^2 + \gamma_{\text{eff}}^2) . \quad (9)$$

Note that the eigenvectors are not normalized to unit length. ξ_0 is parallel to the effective field and corresponds thus to longitudinal magnetization, while $\xi_{\pm 1}$ describe the transverse component precessing around the effective field. The precession frequency Ω is determined by the Larmor frequency Ω_L and the light-shift term $\bar{\Delta} P_+$. The deviation from the Larmor frequency is always positive and largest if the optical detuning is equal to the homogeneous linewidth ($\bar{\Delta} = 1$).

The expansion coefficients c_i are determined by the initial condition. For a sample in thermal equilibrium, the ground-state orientation vanishes, i.e., $\mathbf{m}(0) = 0$. The coefficients are then

$$c_0 = -\frac{\bar{\Delta} P_+^2}{\Omega^2 \gamma_{\text{eff}}}, \quad c_{\pm 1} = \frac{P_+ \Omega_L (\pm i\Omega + \gamma_{\text{eff}})}{2\Omega^2(\Omega^2 + \gamma_{\text{eff}}^2)} . \quad (10)$$

The evolution of the magnetization is shown graphically in Fig. 2 for the parameters $P_+ = 5 \times 10^4\ \text{sec}^{-1}$, $\gamma = 10^4\ \text{sec}^{-1}$, $\Omega_L / 2\pi = -1.5$ MHz, $\bar{\Delta} = -0.1$, and $\bar{\Delta} = 0$. The curved line represents the tip of the magnetization vector tracing out a curve in three-dimensional space. Also shown are the stationary values of the magnetization- $\mathbf{m}_\infty$ and the longitudinal and transverse eigenvectors $c_0 \xi_0$ and $c_1 \xi_1$ -l-c- $_1 \xi_{-1}$. For $\bar{\Delta} \neq 0$, the tip of the magnetization vector moves on the surface of a cone in a spiraling motion towards the apex of the cone which cor-

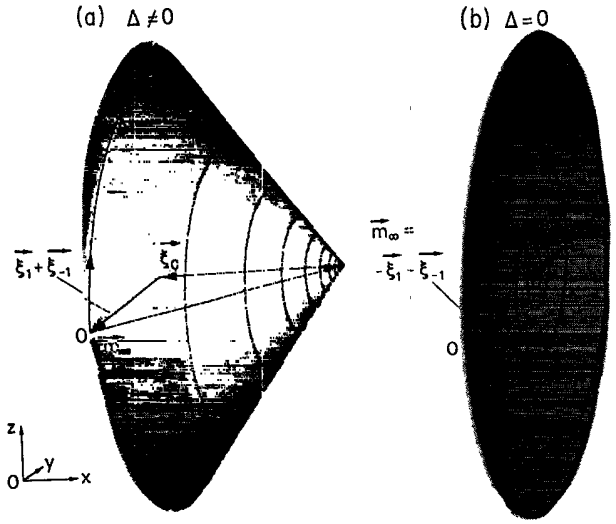

FIG. 2. Evolution of the magnetization under the Hamiltonian described in the text, with (a) off-resonance and (b) on-resonance optical irradiation. The magnetic field is along the x axis, while the virtual field due to the light-shift effect points along the z axis. For $\Delta\neq 0$, the tip of the magnetization vector moves on the surface of a cone towards the stationary value at the tip of the cone. Also shown is the stationary value of the magnetization and the longitudinal (ξ_0) and transverse components ($\xi_1+\xi_{-1}$) of the time-dependent magnetization.

responds to the stationary value of the magnetization. The location of the apex is determined by the system parameters [see Eq. (9)]. The symmetry axis of the cone is parallel to the direction of the effective field $\mathbf{\Omega}$, and the opening angle is determined by the initial condition (in our case the origin O), which must lie on the surface of the cone. If the optical field is applied at exact resonance ($\bar{\Delta}=0$), the virtual field due to the 'light shift vanishes; as shown in Fig. 2(b), the cone collapses in this case to a circle lying in the xy plane.

The graphical representation of Fig. 2 shows again the decomposition of the precessing magnetization into the three components: the stationary value $\mathbf{m}_\infty$ and the exponentially decaying longitudinal and transverse components $c_0\xi_0$ and $c_1\xi_1+c_{-1}\xi_{-1}$. While the stationary value is determined by Eq. (9), the expansion coefficients c_0 and $c_{\pm 1}$ can be calculated from Eq. (10) or via a geometrical procedure suggested by inspection of Fig. 2: c_0 is given as the projection of the nonstationary part of the initial magnetization $\mathbf{m}(0)-\mathbf{m}_\infty$ onto the direction of the effective field $\mathbf{\Omega}=(\Omega_L,0,\bar{\Delta}P_+)$, while the orthogonal component corresponds to the precessing transverse magnetization $c_1\xi_1+c_{-1}\xi_{-1}$.

The motion of the magnetization vector can be compared to the usual Rabi nutation which is a precession of the magnetic moment around an effective field in a frame of reference rotating at the frequency of the irradiation field. Since the optical pulse generates a dc effective field, in our case the spin precession occurs in the (static) laboratory frame of reference. A similar case is known from zero-field magnetic resonance, where dc magnetic field pulses are used for the excitation and detection of spin coherence.[14] In contrast to present work, the dynamics of zero-field magnetic resonance is governed by the homogeneous Bloch equations; this means that the magnetic field pulses can only redistribute existing order, while in our case the optical pumping process creates additional magnetization. Note that the pump term P alone in Eq. (4) would lead to an unphysical situation, where the magnetization of the system would grow without limit. Only the simultaneous presence of $P+$ within the relaxation rate $\gamma_{\rm eff}$ provides a stable solution.

In our experiment, we detect only the component m_z parallel to the direction of the laser beam. The time dependence of this component can be written as

$$m_z(t)=[A_1\cos(\Omega t-\phi)+A_2]e^{-\gamma_{\rm eff}t}+m_{z\infty}\,, \tag{11}$$

$$A_1=\frac{-P_+\Omega_L^2}{\Omega^2(\Omega^2+\gamma_{\rm eff}^2)^{1/2}}\,, \tag{12a}$$

$$A_2=-\frac{\bar{\Delta}^2P_+^3}{\gamma_{\rm eff}\Omega^2}\,, \tag{12b}$$

$$\tan\phi=-\frac{\Omega}{\gamma_{\rm eff}}\,, \tag{12c}$$

$$m_{z\infty}=\frac{P_+}{\gamma_{\rm eff}}\left[1-\frac{\Omega_L^2}{(\Omega_L^2+\bar{\Delta}^2P_+^2+\gamma_{\rm eff}^2)}\right]. \tag{12d}$$

We can thus distinguish three terms via their characteristic time dependence: the first term, originating from the transverse magnetization, oscillates at the frequency Ω and is simultaneously attenuated at a rate $\gamma_{\rm eff}$. The second term, corresponding to the longitudinal magnetization, does not oscillate, but decays at the same rate as the oscillating part, The third, time-independent term corresponds to the stationary ground-state orientation. The evolution of the magnetization component m_z as a function of time is shown graphically in Fig. 3(a). The relevant parameters used for the calculation are $\bar{\Delta}=2$, $P_+=2\times10^5\ \mathrm{s}^{-1}$, $\Omega_L/2\pi=318$ kHz, and $\gamma=3.3\times10^4\ \mathrm{s}^{-1}$. The solid line represents the magnetization component $m_z(t)$ as a function of time; the second term of Eq. (11), i.e., the contribution from the exponentially decaying longitudinal magnetization, is depicted separately by the dashed curve. The precession of the transverse magnetization is seen as an oscillation superimposed onto the exponential background. The final value is determined by the stationary term $m_{z\infty}$.

With the parameters chosen, we have $\Omega/\gamma_{\rm eff}=19.9\gg 1$ and therefore $\phi\approx\pi/2$ [see Eq. (12c)]. The oscillating component has thus a sine characteristic, as can be clearly seen in Fig. 3. This is typical for low-power irradiation, while high-power irradiation near resonance ($\bar{\Delta}\approx 0$) affects the decay rate but not the effective field and results in $\phi\approx 0$ i.e., a cosine characteristic. These features are sometimes not directly apparent in the experimental time-domain signal, where the superposition of the nonprecessing exponential background and the oscillating component make it difficult to extract the phase information. It is then useful to Fourier transform the data, as shown in Fig. 3(b). The solid line represents the real part of the Fourier transform (i.e., the cosine trans-

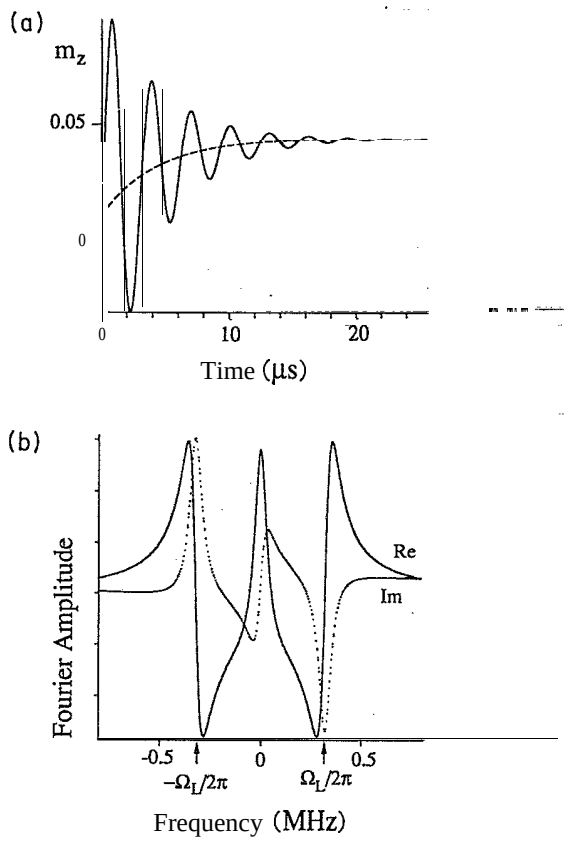

FIG. 3. (a) Calculated time dependence of the magnetization component m_z for the parameters $\bar{\Delta}=2$, $P_+=2\cdot10^5\,s^{-1}$, $\Omega_L/2\pi=318$ kHz, and $\gamma=3.3\times10^4\,s^{-1}$. (b) Fourier transform of the same data in arbitrary units. The solid line represents the real part, the dotted line the imaginary part. The arrows indicate the Larmor frequency.

form), while the dotted line corresponds to the imaginary part (i.e., the sine transform). In the frequency domain, the oscillating component appears as a resonance line around $\pm\Omega/2\pi$, while the contribution of the longitudinal magnetization leads to a resonance line near zero. The shape of the resonance lines are good indicators for the phase. The resonance line near zero frequency has an absorptionlike appearance in the real part of the spectrum and a dispersionlike feature in the imaginary part. The resonance line near $\Omega/2\pi$ appears dispersionlike in the real part and absorptionlike in the imaginary part, a clear indication that the phase is close to $\pi/2$.

The two terms of Eq. (12d) have a straightforward interpretation: the first term $P_+/\gamma_{\rm eff}$ is the ground-state orientation as it would result from optical pumping in the absence of a magnetic field. The second term is therefore the modification due to the precession around the tilted effective field. The presence of the magnetic field leads thus always to a decrease of the ground-state orientation; in the limit of strong magnetic fields $\Omega_L^2 \gg \bar{\Delta}^2 P_+^2, \gamma_{\rm eff}^2$, the stationary value of the z magnetization vanishes. This can easily be seen by a physical consideration: for strong magnetic fields, the spins precess around an axis that is essentially parallel to the direction of the magnetic field (the x axis), while the optical pumping process generates additional polarization along the direction of the laser beam (the z axis). Since the Larmor precession is fast compared to the optical pumping process, the magnetization is spread out in the yz plane faster than it is created, leading to a vanishing overall magnetization.

Not only the precession frequency, but also the decay rate depends on the optical pump rate, since the optical pumping process destroys the ground-state coherence. This dependence of the spin relaxation of optically polarized Na atoms on light intensity is well known from optical-pumping experiments using broadband excitation.[15] The longitudinal and the transverse component of the transient magnetization both decay with the effective decay rate

$$\gamma_{\rm eff}=\gamma+P_+=\gamma+\frac{|\beta_+|^2}{\Gamma_2(1+\bar{\Delta}^2)}\ . \tag{13}$$

In the frequency domain, this relaxation rate corresponds to a broadening of the resonance which is largest on optical resonance ($\bar{\Delta}=0$).

IV. DETECTION OF SUBLEVEL COHERENCE

The ground-state magnetization can be detected via its influence on the optical properties, i.e., the susceptibility of the sample. Due to the optical pumping, the sample is in an anisotropic state, so that the absorption coefficient α depends on the polarization of the light; we use the indices plus and minus to label the coefficients for right and left circularly polarized light, respectively. They depend on the polarization m_z of the medium as[11]

$$\alpha_\pm=\alpha_0(1\pm m_z)\ , \tag{14}$$

where α_0 represents the absorption coefficient of the unpolarized medium. This can most easily be understood by considering Fig. 1. Since $\sigma_+(\sigma_-)$ light probes the transition $|1\rangle\leftrightarrow|4\rangle(|2\rangle\leftrightarrow|3\rangle)$, it is affected only by atoms in the state $|1\rangle(|2\rangle)$. The fraction of atoms in this particular substate is $(1+m_z)/2[(1-m_z/2]$, so that the optical properties of the sample, which are assumed to be linear in the particle number, have to be weighted by the corresponding factors.

The complex amplitude of the probe laser beam entering the test region may be written in terms of these polarizations. We write $E_+(0)[E_-(0)]$ for the real amplitude of the right (left) circularly polarized light. After passing a distance ℓ through the sample, the amplitude of the plus component becomes

$$E_+=E_+(0)e^{-\alpha_+\ell/2}\ , \tag{15}$$

and for the minus component accordingly. The intensity difference AI between left and right circularly polarized light after the sample is given as

$$\Delta I=\frac{E_0^2}{c\varepsilon_0}e^{-\alpha_0\ell}\sinh(m_z\alpha_0\ell)\ . \tag{16}$$

For small signals, i.e., $m_z\alpha_0\ell \ll 1$, it is useful to expand this expression in a power series with respect to m_z. Since all even-order terms vanish, the linear term

$$\Delta I_1 = m_z \left[-\frac{E_0^2}{c\varepsilon_0} e^{-\alpha_0 \ell} \alpha_0 \ell \right] \tag{17}$$

will often be a good approximation for the exact signal. Apparently, this detection scheme allows a direct measurement of the polarization component m_z via the change in the differential absorption profile. It is background-free and the resulting signal is directly proportional to the polarization m_z, weighted with the absorption coefficient α_0 times the interaction length ℓ of the sample and attenuated by the absorption of the isotropic sample $e^{-\alpha_0 \ell}$.

The presence of the magnetization m_z modifies not only the absorption properties of the sample, but also the dispersion. Alternative detection schemes utilizing the different dispersion for left and right circularly polarized light are possible and have been used.[5] The dispersive detection scheme is advantageous if measurements are to be performed far from resonance, since its sensitivity drops off more slowly as a function of optical detuning, while the absorptive scheme allows measurements near the center of the resonance line.

V. EXPERIMENTAL RESULTS AND DISCUSSION

Our experiments were performed on the Zeeman sublevels of the $^2S_{1/2}$ ground state of at omic sodium in an argon atmosphere with a pressure $P_{Ar}=210$ mbar. The Na sample was placed in a ceramic tube which was heated over a length of 6 cm. The D_1 line ($\lambda=589.6$ nm) was used for optical excitation. Figure 4 shows a schematic representation of the experimental setup. The pump beam and the detection beam were derived from the same cw ring-dye laser (Spectra-Physics, model 380D), stabilized with a model 389 stabilock system. The short-term laser linewidth was < 500 kHz. The laser beam was split into pump and probe beam. The pump beam was circularly polarized; the pulses were formed by an acousto-optic modulator (Isomet 1205C) with a rise time of 10 ns. The probe beam was linearly polarized and passed through the sample at an angle of 0.5° with respect to the pump beam. The total power of th.e probe beam was 0.2 mW and the diameter at half-intensity 1.1 mm; at this intensity the damping of the spin coherence due to optical pumping by the probe beam is negligible compared with the decay due to diffusion. An arrangement of three orthogonal Helmholtz coils was used to compensate the earth magnetic field and to generate the transverse field in our experiments in the vertical direction. The resulting field of 32.6 μT lead to a Larmor frequency of $\Omega_L/2\pi=228.5$ kHz, corresponding to the Landé factor $|g_F|=0.5$ Behind the sample, the pump beam was blocked, while the probe beam was passed through a $\lambda/4$ plate and a subsequent beam splitter. Each of the partial beams was passed through an analyzer plate and focused onto a photodiode. With appropriately oriented analyzer plates, the current of the two photodiodes is proportional to the intensity of the right and left circularly polarized component of the probe beam emerging from the sample. The currents of the two diodes were subtracted, amplified, and recorded on a digital storage oscilloscope (LeCroy model 9400) from where it was subsequently transferred to a Macintosh II computer for data analysis and storage.

The signals were recorded at a cell temperature of 175 °C. The small signal absorption at the line center was 20%. From the absorption profile, we calculated a particle density of 4.5. $10^9\,\mathrm{cm}^{-3}$; in our probe volume, the total number of atoms was thus some 2.5×10^8. The buffer gas caused a pressure broadening of the optical resonance line to a half-width at half-maximum (HWHM) of 2.2 GHz. While the absorption line looks almost symmetric under visual inspection, the pressure broadening of 1.25 GHz (HWHM) is not much larger than the Doppler broadening (0.85 GHz, HWHM) or the hyperfine splitting (1.8 GHz) of the ground state. The homogeneously broadened $J=\frac{1}{2} \leftrightarrow J'=\frac{1}{2}$ transition of our theoretical model is thus only a rough approximation for the complicated level structure of sodium.

The resonance detuning of the laser frequency was set from the computer via the external scan input of the laser stabilizing electrons; a Na vapor cell without buffer gas served as the frequency reference and a scanning Fabry-Perot was used to calibrate the scan range. For every experiment, the laser frequency was set to the desired detuning from the absorption maximum of the Na reference cell. In addition to the pressure broadening, the Na reso-

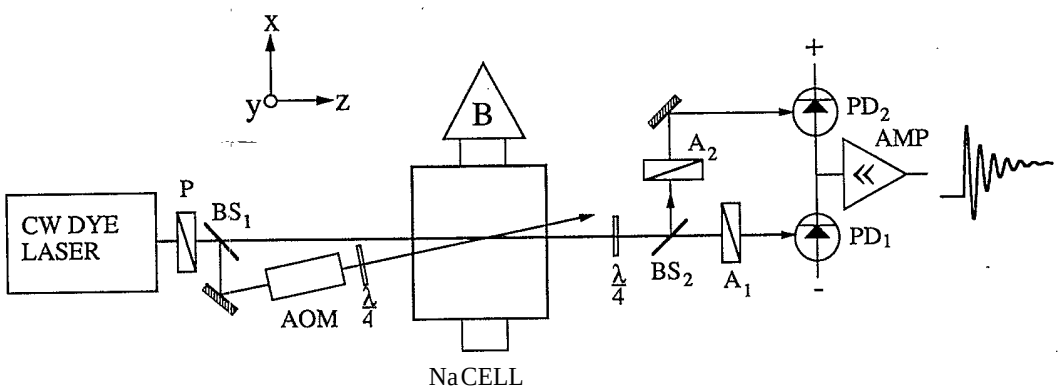

FIG. 4. Experimental setup for the measurement of optically induced spin nutation via absorption measurements. BS_1, BS_2; beam splitters; AOM: acousto-optic modulator; $\lambda/4$: retardation plate; P, A_1, A_2: polarizers; PD_1, PD_2: photodiodes; B: magnetic field.

nance in the sample cell was also shifted towards the red by 0.5 GHz by the interaction with the Ar buffer gas. This frequency shift was determined from simultaneous absorption spectra of the reference cell and the experimental sample cell. The detuning values given with the experimental results refer to the absorption maximum of the sample cell.

Some typical results for the dynamic response of the sample at different pump powers are shown in Fig. 5. Since the beam diameter was 1.1 mm, the laser powers given in the figure in mW correspond approximately to average intensities measured in $kW\,m^{-2}$. The corresponding Rabi frequencies are $<10^8\,s^{-1}$, well below the optical saturation intensity. The signals were recorded with the laser tuned 1.5 GHz below resonance. When the laser field is switched on, the sublevel polarization starts to build up and at the same time precesses around the effective field. At low laser intensities, the resulting polarization is small, while higher laser intensities not only lead to a higher equilibrium polarization, but also to a stronger damping of the transient nutations. At the same time, the increase in laser intensity should also lead to an increase in the precession frequency. Since this effect is relatively small and obscured by the associated damping, the increase in the precession frequency is not readily seen in these figures. All the measurements presented here were performed with Gaussian laser beams, so that the laser intensity was not homogeneous over the sample. As a result, the damping of the oscillations by the optical pumping leads to a nonexponential decay of the signal, with the signal components from the center of the pump beam decaying faster than the signal contributions from the regions with lower intensities.

Figure 6 shows the Fourier transform spectra of the absorption signals; the solid line represents the real part of the complex transform (i.e., the cosine transform), the lower curve the imaginary part (the sine transform). This representation allows one to readily distinguish between the different signal components: the transverse (oscillating) component leads to resonance lines at the frequency $\pm\Omega$, while the longitudinal component appears as a signal near zero frequency. Both components decay exponentially and the width of these signals is proportional to the decay rate of the corresponding magnetization components. From our theoretical results, we expect that both components should decay at the same rate. While the overlap between the signals does not allow an exact measurement, it is evident that the width of both

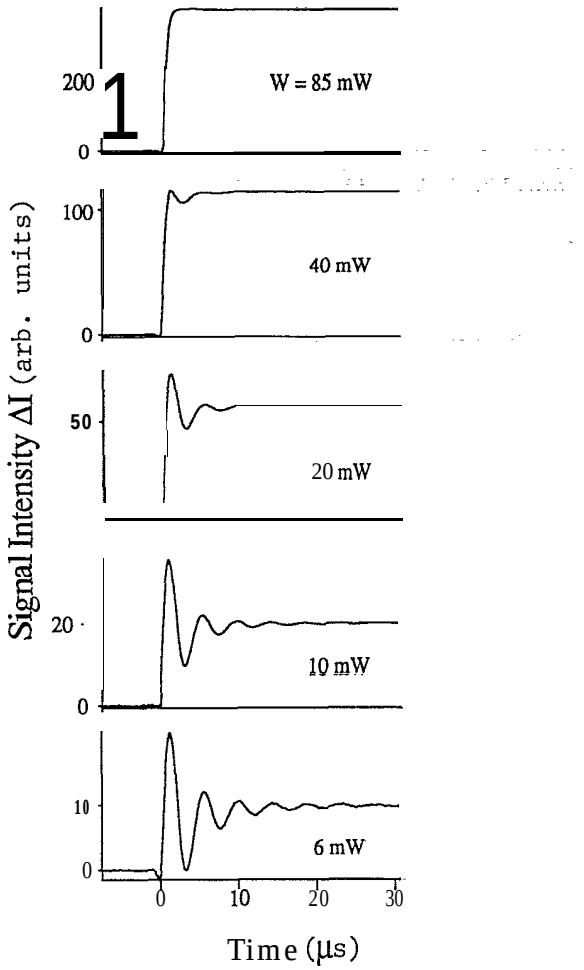

FIG. 5. Measured differential absorption AI of the sample as a function of pump beam power W. The data were recorded at a resonance detuning of $\Delta/2\pi = -1.5$ GHz.

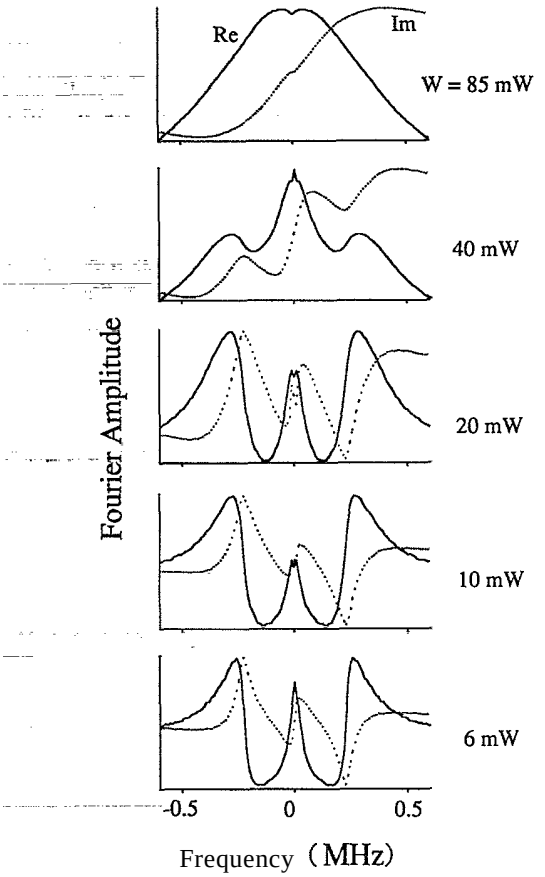

FIG. 6. Real and imaginary part of the Fourier transforms of the data in Fig. 5. The amplitudes are not normalized. For details see text.

resonances is comparable and both become broader as the laser power is increased. Also visible is a slight variation in the phase of the precessing component, as predicted by Eq. (12).

The dependence of the nutation signal on the optical detuning is shown in Figs. 7 and 8. The signals were recorded with 20 mW pump power. Figure 7 contains again the time-domain signals, while the frequency-domain spectra are shown in Fig. 8. From our theory, we expect that the observed signals should not depend on the sign of the optical detuning; experimentally we observe a small asymmetry of the signal amplitude which we tentatively assign to the unresolved hyperfine structure of the optical transition. We will restrict ourselves therefore to measurements recorded with the laser detuned to the red. As the detuning is increased, the pump rate is reduced and the signal intensity and the magnetization decay rate are decreased. The Fourier transform data in Fig. 8 also show the expected behavior. Since the light-shift contribution to the effective field vanishes on resonance, the effective field is parallel to the x axis and the nonprecessing contribution to the signal vanishes. At larger detunings ($\bar{\Delta} \approx 1$), the effective field tilts towards the z axis and the exponential background becomes the dominant part of the signal (see Fig. 8). When the detuning is increased even further, the pump rate decreases and the effective field returns towards the x axis. Close to resonance, the phase of the precessing term is determined by the ratio of the Larmor frequency to the pump rate ($\tan\phi \approx -\Omega_L / P_+$), while it tends towards 90° far from resonance ($\tan\phi \approx -\Omega_L / \gamma \approx -7$). Again, it can readily be seen that both signal components decay at approximately the same rate.

Figure 9 shows the nutation signals calculated with Eqs. (11) and (12) for the same parameter values as the experimental curves in Fig. 7. Apart from the overall amplitude for all four spectra, no adjustable parameters have been used for this calculation. The agreement between the theoretical prediction and the experimental results is quite good, which is very satisfying in view of our rather simple model. The largest discrepancy is in the amplitude of the signal at -3.5 GHz.

The decay rate as a function of detuning Δ has been analyzed quantitatively; the results are shown in Fig. 10. The numerical analysis of the experimental data is complicated considerably by the inhomogeneous intensity profile of the laser beam which leads to a nonexponential decay. It is therefore impossible to uniquely determine a damping rate from the experimental data without measuring the beam profiles of both pump and probe beam, the overlap geometry of both laser beams and the particle density, and using a sophisticated fitting procedure. We have chosen to use a much simpler procedure which still allows us to determine whether there is at least a qualitative agreement between theory and experimental results; the nutation signals were Fourier transformed and the width of the resulting resonance line was taken as a measure of the decay rate. The horizontal axis in Fig. 10 represents the detuning-dependent reduction of the optical-pump rate, while the vertical axis cor-

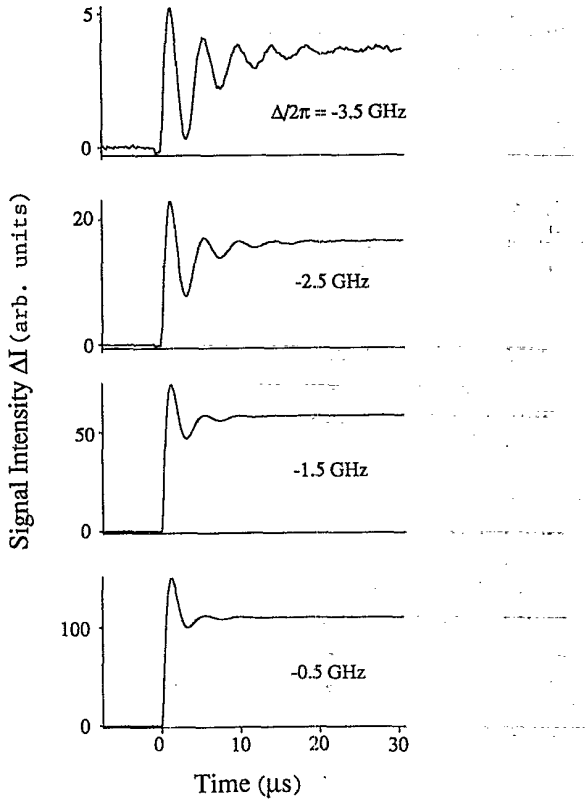

FIG. 7. Measured differential absorption ΔI of the sample as a function of resonance detuning $\Delta/2\pi$. The data were recorded at a pump beam power of 20 mW.

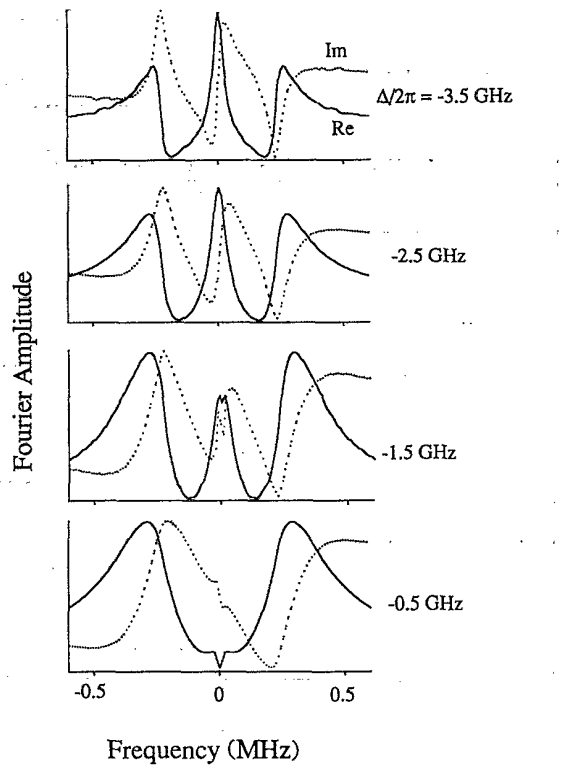

FIG. 8. Fourier transforms of the data in Fig. 7. The amplitudes are not normalized. For details see text.

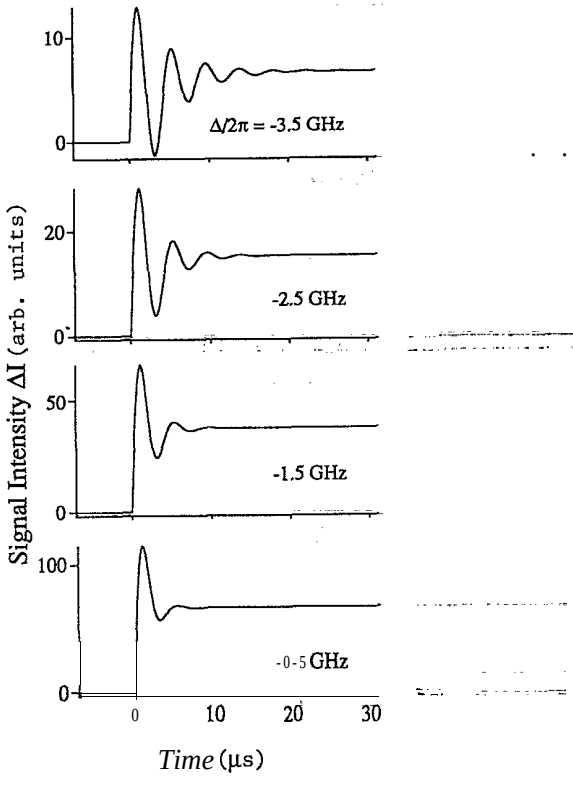

FIG. 9. Calculated spin transients for various optical detunings A, corresponding to the experimental data in Fig. 7. The parameter values are $|\beta|^2/\Gamma_2 = 7.91 \times 10^5\,s^{-1}$, $\Omega_L/2\pi = 228$kHz, $\gamma = 3.3 \times 10^4\,s^{-1}$.

responds to the decay rate of the magnetization. The experimental data points are compared to the theoretically predicted straight line. The intersection of this line with the y axis is determined by the point at vanishing pump intensity. This latter value was determined in a separate measurement by switching off the pump beam after a steady-state magnetization was established, and measuring the decay rate in the absence of optical pumping. The slope of the theoretical curve was determined by a least-squares fit for the optical Rabi frequency β_+. In view of the difficulties mentioned above, the agreement between theory and experimental results is quite satisfactory.

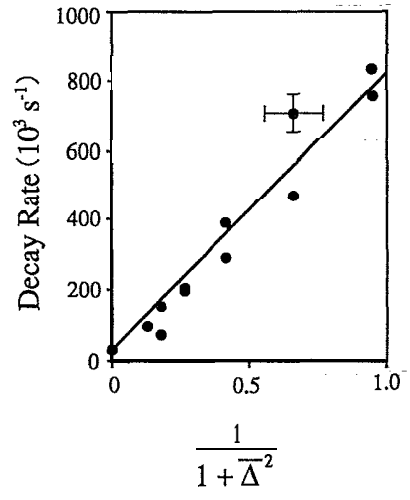

FIG. 10. Decay rate of the initial transient as a function of the resonance detuning for a fixed pump beam power. The circles represent experimental data, while the straight line is the theoretical prediction.

Our results on the evolution of the ground-state polarization have some practical implications for the experimentalist who wants to polarize the ground state by optical pumping to the largest extent possible. In the limit of low laser power, i.e., if the optical pump rate $P+$ falls below the Larmor frequency Ω_L, the evolving magnetization shows pronounced oscillations as a function of time (see Fig. 5). Since the amplitude of these oscillations is larger than the stationary value of the magnetization by a factor of order Ω_L/P_+, it is advantageous to sample the magnetization not in the steady state, but at the peak of the oscillation which is reached after a time $\pi/2\Omega_L$. In the case of strong irradiation, on the other hand, the oscillatory component is small; the magnetization quickly reaches an equilibrium value and remains constant thereafter.

With the quantization axis parallel the static magnetic field, the ground-state orientation m_z (i.e., along the laser beam) appears as coherence between the ground-state sublevels that is induced by a resonant two-photon transition of the Raman type. In this representation, the relationship of our experiments to the well-known coherent Raman beats becomes obvious: in the latter case, the oscillations are observed in coherently prepared molecular samples when the level degeneracy is suddenly removed by Stark-pulse switching;[16] the laser and the Raman light then propagate together and produce a coherent beat with a frequency that corresponds to the level shift induced by the Stark-pulse switching. In our case, the transient coherence between the nondegenerate Zeeman sublevels is induced by a step input of light; the time evolution of the driven spin system is then observed in forward scattering of an optical probe beam using polarization selective detection. With this technique, we have measured in detail the effect of off-resonance excitation and of light intensity on the spin nutation, with special emphasis on the dephasing time, the amplitudes of the different magnetization components, and the signal phase. In this respect, our work extends previous experiments on coherent Raman beats.

Related nutation signals were also observed in Doppler-free two-photon excitation in a ladder-type three-level system." Since the two-photon method excites all the atoms with the same energy detuning, it makes it possible to study off-resonance transients. The sudden irradiation of atoms allows the observation of ringing phenomena corresponding, however, to optical nutation. In our case, the initial and final state are only separated by energies corresponding to radio frequencies. – Our work can also be compared to previous studies on sublevel transients in optically excited states where the situation of a low-power excitation pulse being long compared to the Zeeman precession period was investigated in fluorescence.*' It was observed that the modulation

depth of the final transient ("quantum beat signal") was modulated in dependence of the excitation pulse length. This behavior can be easily understood by inspection of our Fig. 5: for low-power pulses with durations on the time scale of the initial transient, the sublevel coherence or spin orientation shows pronounced oscillations. Thus, if the excitation pulse length is varied on the time scale of the initial transient, the amplitude of the subsequent free induction decay signal will show the same oscillatory behavior.

Finally, our findings can be related to radio-frequency experiments. Here it is well known that if one suddenly applies a radio-frequency field to nuclear spins, it is possible to observe oscillations at the generalized Rabi frequency including the resonance detuning from the sublevel splitting frequency.[19] In our work, the effective field is the combination of a magnetic field and a pseudo magnetic field due to the light-shift effect.

VI. CONCLUSIONS

In summary, we have reported experimental and theoretical investigations of the dynamics of an atomic ground-state spin system in response to a step input of light. The complete time evolution of the initial transient was investigated as a function of optical resonance detuning and laser intensity; due to the strong pressure broadening of the Na D_1 line, excited-state effects could be neglected and the dynamics of the ground-state spin system could be isolated. In addition, the pressure broadening allows us (within limitations) to disregard the hyperfine structure of the Na ground state and use a simple model of the spin dynamics. Our experiments extend previous work on optically driven spin transients as they are performed with long, narrow bandwidth pulse excitation and are not restricted to the limit of impact excitation and broadband excitation being generally imposed by the use of short excitation pulses.

Our findings have some practical implications for the experimentalist aiming to create the largest possible ground-state polarization with optical pulses of variable length or intensity. The measurements have also shown that in the saturation limit a large spin coherence can be optically induced even under stationary conditions. The pronounced dependence of the length and orientation of the steady-state spin polarization on the laser intensity is reflected in the amplitude and phase of the free induction decay signal following the end of the excitation pulse.[6] As we have seen, the fictitious magnetic field due to Zeeman light shifts can play an important role in the dynamics of optically pumped electron spins. Since this fictitious field is oriented along the direction of the laser beam, which in our case is orthogonal to the magnetic field direction, it can be used to invert the phase of spins precessing in the magnetic field. For an ensemble of spins in an inhomogeneous magnetic field, an optical pulse can thus create a spin echo.[6,20]

Our results are also of interest for sublevel spectroscopy using pump-probe techniques in combination with ultrashort laser pulses; such sublevel transients can now be observed on a picosecond time scale with potential applications not only in gases but also in liquids and solids.[21] Although our experiments are performed on a much slower time scale of some 10 μs, similar signal features as reported here should also be present for optically driven sublevel transients on ultrashort time scales, provided the dephasing times of the optical dipoles is short compared with the laser pulse duration or coherence time.

Although a simple model based on a Bloch-type equation for the ground-state spin polarization of Na is used, our theoretical predictions are in good qualitative agreement with the experimental observations. Strictly speaking, the present results apply only for a $J=\frac{1}{2}$ to $J'=\frac{1}{2}$ atomic system. However, the observed signal features of optically driven sublevel transients are likely to occur also for other level schemes, provided that comparable experimental conditions are met. The situation will be different as soon as optical coherences or excited-state effects become important; obviously this will be the case if transient spin phenomena are created in optically excited states. With respect to atomic ground states our results contribute to a better understanding of optically driven sublevel transients and may prove useful whenever this technique or related optical methods are applied to gather spectroscopic information on relaxation parameters and splitting frequencies of sublevel resonances.

ACKNOWLEDGMENTS

This work was supported by the Schweizerischer Nationalfonds. One of the authors (J.M.) acknowledges helpful discussions with C. Cohen-Tannoudji.

[1]See, e.g., A. Kastler, Science **158**, 214 (1967), and references therein.

[2]Y. R. Shen, The ***Principles of Nonlinear Optics*** (Wiley, New York, 1984), p. 57.

[3]See, e.g., S. Haroche, ***High Resolution Laser Spectroscopy***, edited by K. Shimoda (Springer, Heidelberg, 1976), p. 253, and references therein.

[4]See, e.g., J. Mlynek and W. Lange, Opt. Comm. 30, 337 (1979); R. M. Shelby, A. C. Tropper, R. T. Harley, and R. M. Macfarlane, Opt. Lett. 8, 304 (1983); T. Kohmoto, Y. Fukuda, M. Tanigawa, T. Mishina, and T. Hashi, Phys. Rev. B 28, 2869 (1983); R. M. Lowe, D. S. Gough, R. J. McLean, and P. Hannaford, Phys. Rev. A **36**, 5490 (1987).

[5]For a preliminary report, see S. Burschka and J. Mlynek, Opt. Commun. 66, 59 (1988).

[6]J. Mlynek, M. Rosatzin, and D. Suter, in ***Coherence and Quantum Optics 6***, edited by E. Wolf, L. Mandel, and J. Eberly (Plenum, New York, in press).

[7]J. Dupont-Roc, N. Polonsky, C. Cohen-Tannoudji, and A. Kastler, Phys. Lett. **25A**, 87 (1967); C. Cohen-Tannoudji and

J. Dupont-Roc, Phys. Rev. A 5,968 (1972).
[8]See, e.g., H. Harde and H. Burggraf, Opt. Commun. 40, 441 (1982); T. Mishina, M. Tanigawa, Y. Fukuda, and T. Hashi, Opt. Commun. 62, 166 (1987).
[9]Y. Fukuda, K. Yamada, and T. Hashi, Opt. Commun. 44,297 (1983).
[10]R. P. Feynman, F. L. Vernon, and R. W. Hellwarth, J. Appl. Phys. 28, 49 (1957).
[11]F. Mitschke, R. Deserno, W. Lange, and J. Mlynek, Phys. Rev. A 33, 3219 (1986).
[12]H. G. Dehmelt, Phys. Rev. 105, 1924 (1957).
[13]F. Bloch, Phys. Rev. 70,460 (1946).
[14]R. Kreis, D. Suter, and R. R. Ernst, Chem. Phys. Lett. 118, 120 (1985); J. M. Millar, A. M. Thayer, A. Bielecki, D. B. Zax, and A. Pines, J. Chem. Phys. 83,934 (1985).
[15]H. G. Dehmelt, Phys. Rev. 105, 1487 (1957).
[16]R. G. Brewer and EL. Hahn, Phys. Rev. A 8,464 (1973); Van Stryland and R. L. Shoemaker, Phys. Rev. A 20, 1376 (1979).
[17]M. Bassini, F. Biraben, B. Cagnac, and G. Grynberg, Opt. Commun. 21,263 (1977).
[18]H. Lundberg and S. Svanberg, Opt. Commun. 27,235 (1978).
[19]See, e.g., A. Abragam, *The Principles of Nuclear Magnetism* (Oxford University Press, Oxford, 1978).
[20]M. Rosatzin, D. Suter and J. Mlynek (unpublished).
[21]See, e.g., I. A. Walmsley, M. Mitsunaga, and C. L. Tang, Phys. Rev. A 38, 4681 (1988), and references therein.